Electrochemical and surface studies of the effect of naphthalene-based additives on tin electrodeposition

Aranzales Ochoa, D.M.

CHAPTER 5

The effect of naphthalene-based additives on tin electrodeposition on an iron electrode: an industrial approach

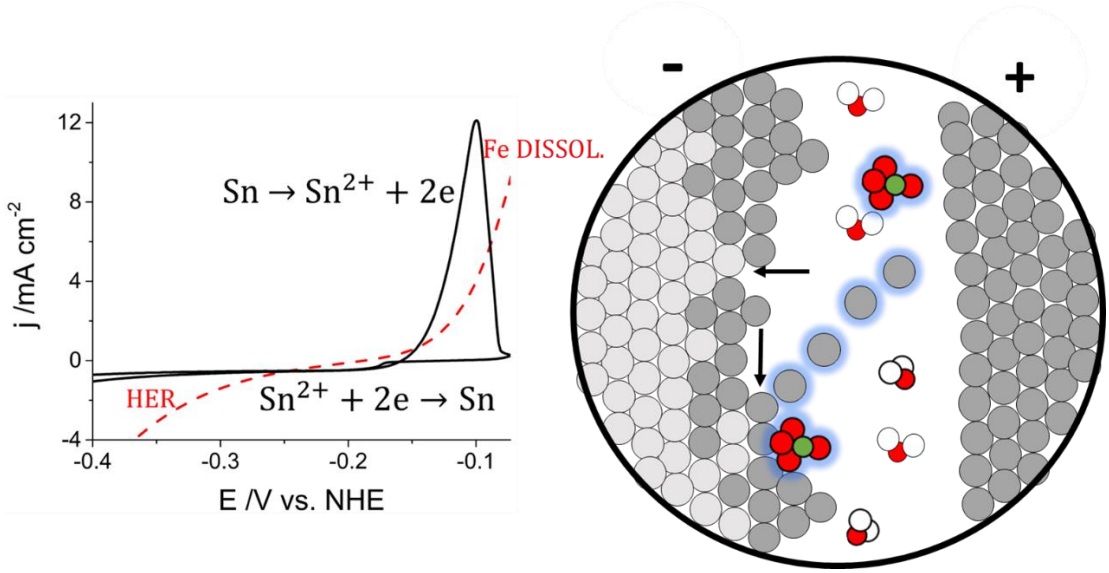

Abstract

In this chapter, we describe preliminary measurements of the effect of naphthalene-based additives on tin electrodeposition on an iron electrode in sulfuric acid media. Considering the highly reactive and complex nature of the iron electrode surface, these measurements aim to compare and use the gathered knowledge of our previous studies of the effect of naphthalene-based additives on tin electrodeposition on more stable substrates, i.e., gold and boron doped diamond electrodes, to provide insights of the interaction of the additives with iron and their effect on the overall tin deposition process on an iron electrode.

Naphthalene-based additives showed to strongly affect tin electrodeposition on iron under acidic media. In the case of NPT and NPTS, tin electrodeposition remains mainly independent of the substrate, NPT and NPTS molecules presumably arrange in a similar way as on a gold surface, since they interact with the substrate mainly via Van der Waals forces. A more compact film of NPTS molecules is formed on the iron substrate since a strong decrease of tin electrodeposition is observed in comparison to NPT. HNPTS stronger decreases the tin deposition, which is in agreement with our observations of its effect on tin deposition on a BDD electrode. Furthermore, we showed that Sn (II) ions transport from the bulk to the electrode surface is not affected by NPT, NPTS and HNPTS but ENSA-6, which exhibits a strong decrease of Sn (II) ions on the surface, presumably due to a slow mass transport of the ions through the ENSA film formed on the electrode surface. Furthermore, ENSA-6 also highly inhibits tin deposition process.

5.1 Introduction

Tin electroplating process finds application as an alloy or coating, and therefore tin plays an important role in daily life, being used in food packaging, jewellery, and also in modern technology [1]. One of the most traditional and important applications of tin electroplating is the protection of iron or steel from air oxidation and the enhancement of their corrosion resistance [12]. Few studies have aimed to understand the effect of industrial additives on the tin deposition process on iron [3]. The main purpose of the present chapter is to use the gathered knowledge of the effect of naphthalene-based additives on tin electrodeposition process on more stable substrates such as gold [4] and boron doped diamond [5] and compare it to the phenomena observed on the tin electrodeposition on an iron electrode, a highly reactive surface.

5.2 Experimental details

Before each measurement all glassware was stored overnight in a solution of 1g L^{-1} $KMnO_4$ in 0.5 M H_2SO_4. Before use, it was rinsed with water and 30% hydrogen peroxide solution in order to remove permanganate anions and trace impurities. Glassware was boiled in water five times before starting the experiments. The water used to clean glassware and to prepare solutions was demineralized and ultra-filtrated by a Millipore MilliQ system (18.2 MΩ cm). The voltammetric experiments were performed in a three-electrode cell configuration at room temperature using an iron disk as a working electrode (5.0 mm diameter, 4.0 mm thickness purchased from Pine-research) used in the rotating-disk electrode (RDE) setup under hydrodynamic conditions, a gold wire as a counter electrode and RHE as a reference electrode, but all the potentials are reported on the normal hydrogen electrode (NHE) scale. The reference electrode was in contact with the electrolyte via a Luggin capillary and connected to an additional gold wire through a capacitor of 10 µF to filter small currents produced in the RHE electrode and to reduce the noise in measurements at low currents.

The iron working electrode was successively polished with 1.0, 0.3 and 0.05 µm of diamond powder suspension, rinsed and transferred to an ultrasound bath with water during 10 minutes before the measurements. The gold counter electrode was electrochemically etched before each experiment firstly by oxidizing it by applying 10 V during 20 s in 0.1M sulfuric acid, a graphite bar was used as a counter electrode, and subsequently by dissolving the gold hydr(oxides) formed on the counter electrode surface by dipping it in a 6 M HCl solution for 30 s. The experiments were performed using a potentiostat VSP-300 (Bio-logic) and the RDE experiments were performed with an MSR rotating electrode (Pine Research) at a rotation

rate of 1600 rpm. The electrode potential was corrected for Ohmic drop during the measurements by using 85% of the Ohmic resistance measured by electrochemical impedance spectroscopy. Finally, the morphology of the tin deposits on the iron electrode were observed ex situ by scanning electron microscopy SEM. Micrographs were taken using the model JEOL 820 SEM at 15 kV and 0.1 nA. Energy Dispersive X-Ray Spectroscopy (EDS) measurements were taken at 15 kV, the reported percentage of tin was calculated from the average of relative ratio of tin from a line scan measurement of 0.5 µm length, over the tin features.

All solutions were prepared from chemicals with the highest purity commercially available: H_2SO_4 (96% ultrapure, Merck), $SnSO_4$ (≥ 95%, Sigma Aldrich), naphthalene (≥ 99%, Sigma Aldrich), 2-napthalenesulfonic acid sodium salt (99.6%, Sigma Aldrich), sodium thiosulfate (≥ 99.99%, Sigma Aldrich), 4-hydroxy-1-naphthalenesulfonic acid sodium salt (≥ 95 %, Santa Cruz Biotechnology) and ethoxylated α-napthalenesulfonic acid (73.6%, Pulcra chemicals). In the case of ENSA the main impurities are sulfuric acid with 8.7 %, and water with 2.4 %, other impurities were not provided by the supplier. The solutions were deaerated with Argon for 20 min before each experiment and a constant flow of Argon above the solution was kept during all the experiments.

5.3 Results and discussion

Figure 1 shows the scanning electron micrographs of the "bare" iron surface just after the mechanical polishing and ultrasound treatment. Fig. 1a exhibits fissures as a consequence of the mechanical polishing procedure. Fig. 1b shows the surface zoom-in, it exhibits 3D flake-like structures almost over the entire flat surface. EDS measurements show the presence of oxygen in the 3D flake-like structures and also over the iron flat electrode surface with a relative ratio of O: Fe (5.4 ± 0.8 % : 94.6 ± 1.3 %). Furthermore, iron oxides are also visible on the electrode surface since the scanning electron micrographs exhibit brighter zones along the defects and edges of the electrode surface (lower conductivity), in which EDS measurements reveal higher contents of oxygen.

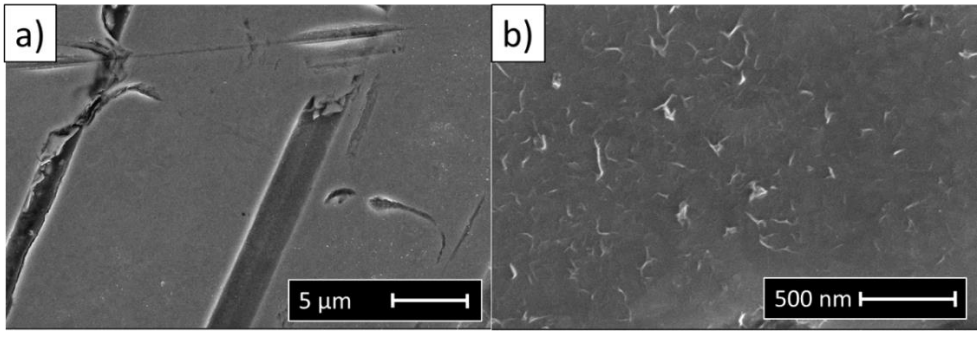

Figure 1. Scanning electron micrographs of the iron substrate 10 minutes after mechanical polishing

Figure 2 shows the cyclic voltammetry of the iron electrode surface in sulfuric acid. Voltammetry recorded shows two different processes: iron dissolution and the hydrogen evolution reaction on the iron surface. From the recorded voltammetry one could say that between -0.15 to -0.35 V the iron surface does not seem very reactive. Nonetheless, the inset of Fig. 1a shows the presence of anodic and/or cathodic currents correlated with iron dissolution and (presumably) hydrogen evolution reaction over the entire potential window. Due to the highly reactive nature of iron substrate under acidic media, no polarizable double layer region is present. Figure 2b shows the Tafel plot of the two processes: hydrogen evolution reaction and iron dissolution. The junction between the anodic and cathodic branches of the Log |j| vs. E is known as the corrosion potential, and its value is -0.274 V. Moreover, Tafel slopes for hydrogen evolution and iron dissolution were obtained, 134 and 48 mV dec^{-1}, respectively, which are mostly in agreement with previously reported values for static conditions [6–9]. Moreover, Figure 3 shows the cyclic voltammetry for iron dissolution and hydrogen evolution reaction on iron electrode under hydrodynamic conditions, a strong increase in the anodic current is observed as a consequence of a strong mass transport effect during iron dissolution process. The values for the Tafel slope for HER is almost identical (137 mV $decade^{-1}$) to the one without rotation, but the Tafel slope changes in the case of iron dissolution (60 mV $decade^{-1}$). Moreover, a shift of the corrosion potential to less negative potentials is also observed (-0.19 V).

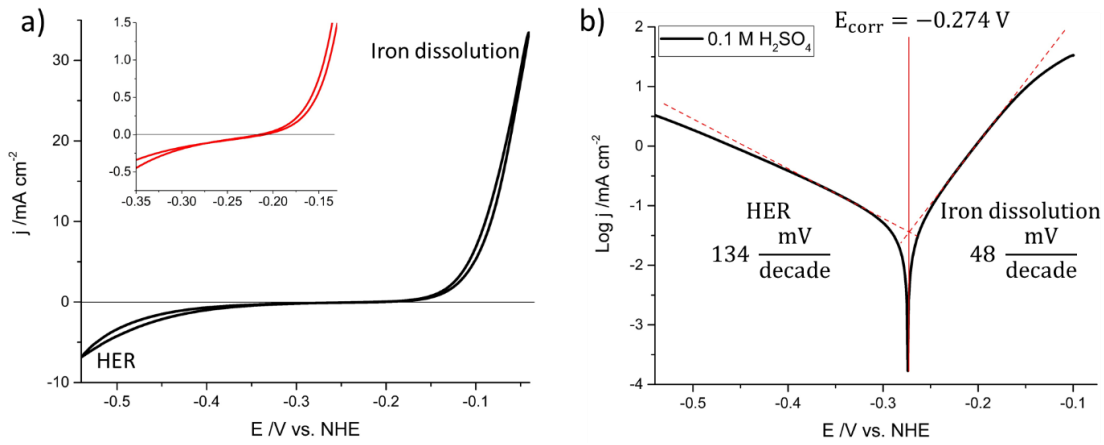

Figure 2. a) Cyclic voltammetry of the iron substrate in 0.1 M H_2SO_4. CV recorded between -0.56 to -0.05 V at 30 mV s^{-1}, static conditions b) Tafel plot for iron electrode in 0.1 M H_2SO_4

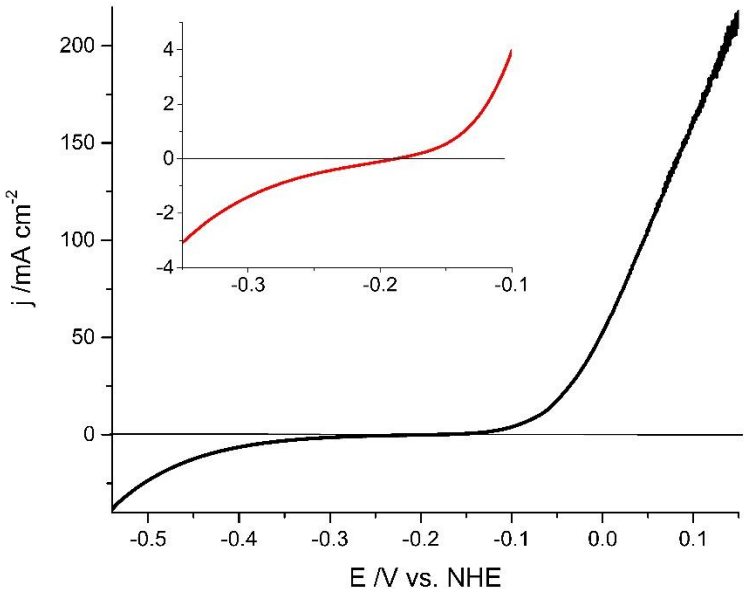

Figure 3. a) Cyclic voltammetry of the iron substrate in 0.1 M H_2SO_4. CV recorded between -0.56 to -0.05 V at 30 mV s^{-1}, under hydrodynamic rotating-disk conditions: 1600 rpm

Hydrogen evolution reaction on iron and iron dissolution processes have been described by the following equations[9]:

Hydrogen evolution reaction steps:

$$H^+ + e^- \leftrightarrow H_{ads}\ (1)\ \text{Rate determining step}$$

$$H_{ads} + H^+ + e^- \leftrightarrow H_2\ (2)$$

$$2H_{ads} \leftrightarrow H_2\ (3)$$

Iron dissolution reaction steps:

$$Fe + H_2O \leftrightarrow Fe\,(H_2O)_{ads}\ (4)$$

$$Fe\,(H_2O)_{ads} \leftrightarrow Fe\,(OH^-)_{ads} + H^+\ (5)$$

$$Fe\,(OH^-)_{ads} \leftrightarrow Fe\,(OH)_{ads} + e^-\ (6)$$

$$Fe\,(OH)_{ads} \rightarrow (FeOH)^+ + e^-\ (7)\ \text{Rate determining step}$$

$$(FeOH)^+ + H^+ \leftrightarrow Fe^{2+} + H_2O\ (8)$$

5.3.1 Tin electrodeposition on an iron electrode

Following our previous studies about the effect of naphthalene-based additives on tin electrodeposition process on gold and boron-doped diamond electrodes[45], we study here the effect of naphthalene-based additives on tin electrodeposition on an iron electrode by means of cyclic voltammetry and ex-situ scanning electron microscopy.

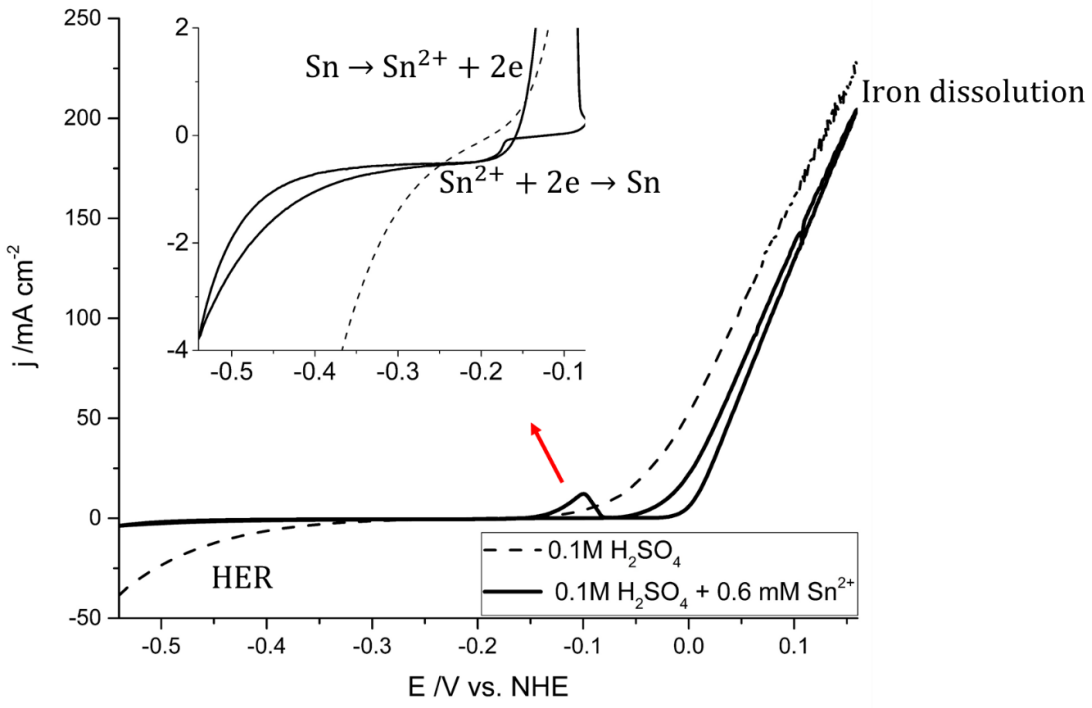

Figure 4. Cyclic voltammetry of tin deposition-dissolution on iron, recorded between -0.54 to -0.16 V at 30 mV s^{-1} and 1600 rpm (Bold line). Cyclic voltammetry of iron dissolution and HER on iron, recorded between -0.54 to -0.16 V at 30 mV s^{-1} and 1600 rpm (Dashed line). Inset of tin bulk deposition and dissolution.

Figure 4 shows the cyclic voltammogram for tin deposition and dissolution on an iron electrode under acidic conditions. In a narrow potential window (~-0.075 to -0.35 V), a cathodic wave at -0.17 V followed by a plateau related with tin bulk deposition under mass transport control at -0.19 V are observed, besides, an anodic peak related with tin dissolution is observed at -0.10 V. Furthermore, from ~-0.35 V to more negative potentials, hydrogen evolution is observed. Since the onset potential is more negative than the HER onset in the blank (see Figure 3), we ascribed it to HER on the tin surface, tin being a bad catalyst for HER. At positive potentials, a shift of the onset potential for iron dissolution to less negative

potentials is observed as a consequence of the tin presence on the iron surface. Furthermore, a decrease in the current density of iron dissolution is also observed.

5.3.2 The effect of naphthalene-based additives on tin electrodeposition on an iron electrode

Figure 5a, 6a and 7a show the cyclic voltammograms for tin electrodeposition and dissolution on an iron electrode in the presence and absence of different concentrations of naphthalene (NPT), naphthalenesulfonate (NPTS) and hydroxynaphthalenesulfonate (HNPTS).

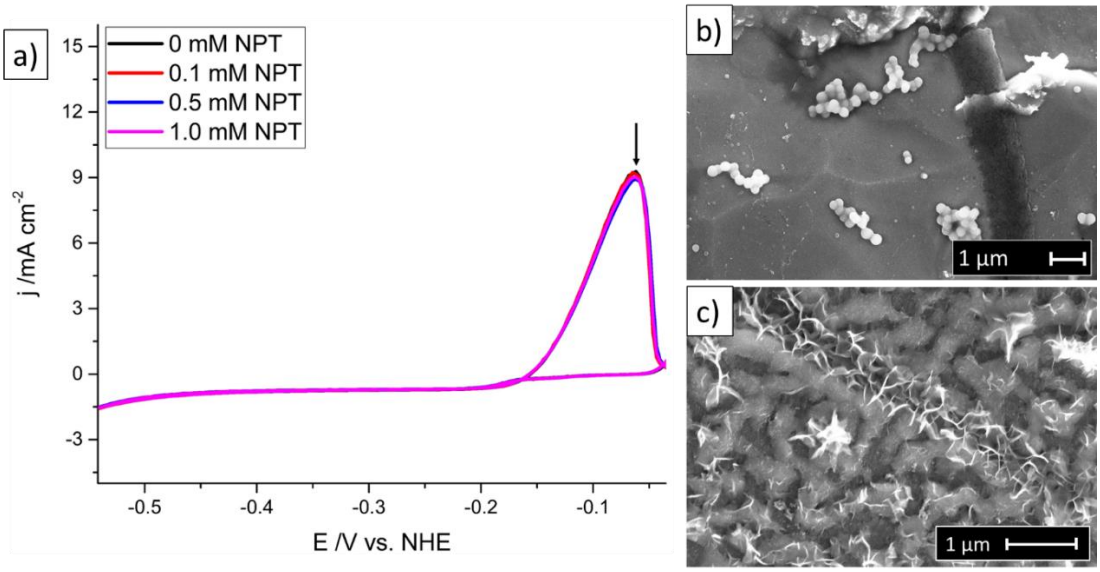

Figure 5. (a) Cyclic voltammograms of tin electrodeposition on a polycrystalline iron RDE, 0.1 M H_2SO_4 at different concentrations of NPT, recorded between -0.541 to 0.1 V and 30 mV s^{-1} and 1600 rpm. SEM micrographs of tin electrodeposited on polycrystalline iron; potential was swept from 0.1 to -0.241 V at 30 mV s^{-1} and 1600 rpm, subsequently the potential was held at -0.241 V during 1 minute, 0.1 M H_2SO_4 , 0.6 mM $SnSO_4$ (b) without NPT (c) with 200 µM NPT

Figure 5a shows almost no effect of NPT on tin electrodeposition – dissolution on an iron electrode in terms of the voltammetric profile, only a very small decrease (if any) in the peak related to the stripping of tin bulk deposited is visible. No remarkable dependence on NPT concentration is observed. Figures 5b and 5c show the scanning electron micrographs of the tin deposits in the absence and presence of NPT, respectively. Unlike Figure 5a, Figures 5b and 5c reveal remarkable differences in the morphology of the tin deposits in the absence and presence of NPT. In the absence of NPT, tin deposits exhibit clusters of spherical tin crystallites almost over the entire surface. The tin crystallites sizes are about 300 nm. In the presence of

NPT, the tin deposit does not show separate tin crystallites, instead a coalesced tin deposit is observed and merges with the 3D – needles of iron oxides.

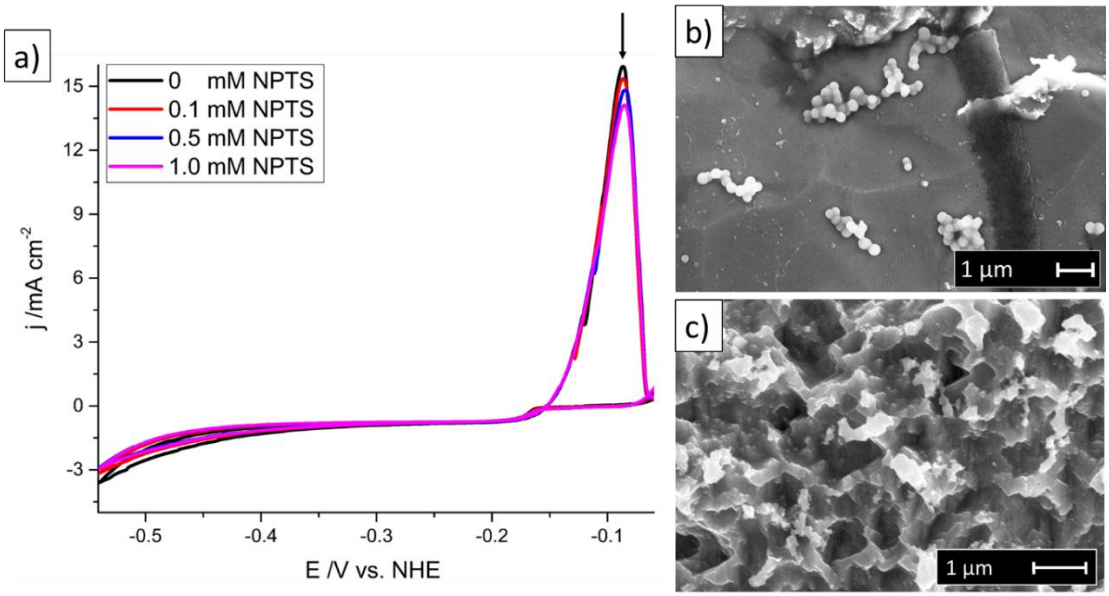

Figure 6. (a) Cyclic voltammograms of tin electrodeposition on a polycrystalline iron RDE, 0.1 M H_2SO_4 at different concentrations of NPTS, recorded between -0.541 to 0.1 V and 30 mV s^{-1} and 1600 rpm. SEM micrographs of tin electrodeposited, on polycrystalline iron; potential was swept from 0.1 to -0.241 V at 30 mV s^{-1} and 1600 rpm, subsequently the potential was held at -0.241 V during 1 minute, 0.1 M H_2SO_4 , 0.6 mM $SnSO_4$, in the presence of: (b) without NPTS (c) with 200 µM NPTS

Figure 6a shows the cyclic voltammogram of tin electrodeposition and dissolution on an iron electrode in the presence of different NPTS concentrations. A small but remarkable decrease of the peak correlated to the stripping of tin bulk deposited is seen in the presence of NPTS, and its decrease seems to be proportional to the increase of NPTS concentration, additionally a slight decrease of hydrogen evolution current is also observed as a consequence of the presence of NPTS. Figures 6b and 6c show that in the presence of NPTS tin deposits do not show well defined crystallites or clusters of crystallites, instead shapeless tin features are concentrated in specific regions of the electrode surface. Figure 6c also shows the presence of 3D layer - network structures on the iron substrate ascribed to iron oxides. Scanning electron micrographs reveal that the substrate morphology is not stable between different measurements, as it is expected due to the highly reactive nature of iron under acidic conditions and oxygen exposure.

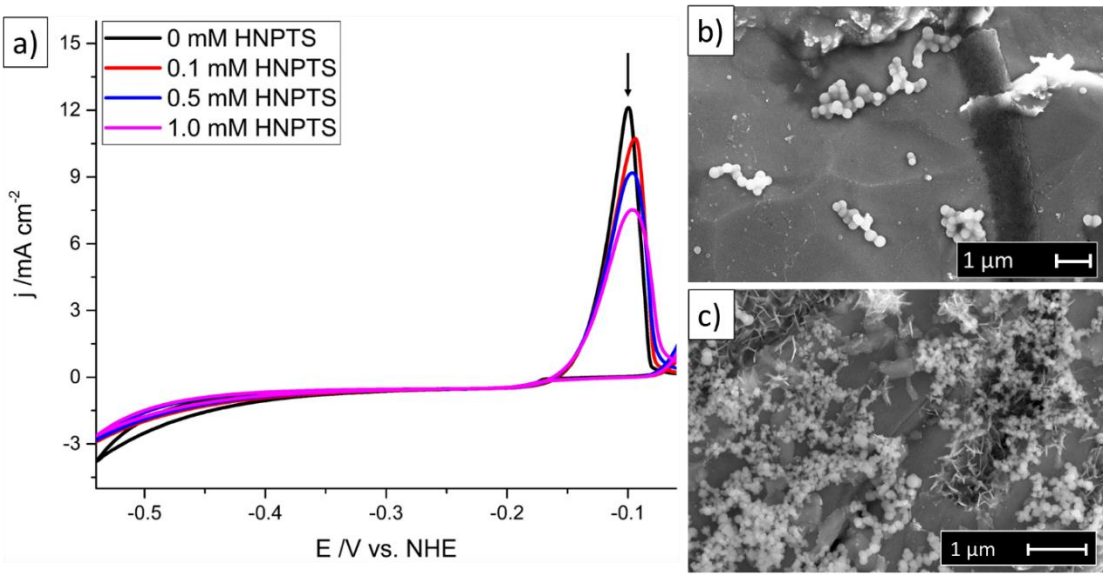

Figure 7. (a) Cyclic voltammograms of tin electrodeposition on a polycrystalline iron RDE, 0.1 M H_2SO_4 at different concentrations of HNPTS, recorded between -0.541 to 0.1 V and 30 mV s^{-1} and 1600 rpm. SEM micrographs of tin electrodeposited, on polycrystalline iron; potential was swept from 0.1 to -0.241 V at 30 mV s^{-1} and 1600 rpm, subsequently the potential was held at -0.241 V during 1 minute, 0.1 M H_2SO_4 , 0.6 mM $SnSO_4$, in the presence of: (b) without HNPTS (c) with 200 µM HNPTS

Figure 7a shows the cyclic voltammogram for tin deposition and dissolution in the presence of HNPTS. A larger decrease in the peak correlated to the oxidation of bulk deposited tin and a slight shift to less negative potentials are observed compared to NPTS. Moreover, a decrease of the hydrogen evolution is also observed. Figures 7b and 7d show the scanning electron micrographs of tin deposits in the absence and presence of HNPTS, respectively. In contrast to the effect of NPT and NPTS on the morphology of tin deposits, tin deposits in the presence of HNPTS do not seem to coalesce, instead spherical tin crystallites are visible, which arrange in clusters similar to the observed morphology of tin deposits in the absence of naphthalene-based additives. A decrease in the size of tin crystallites is seen: crystallites of about 100 nm are present in the clusters. Moreover, Fig. 7c also shows the 3D-flake-like iron oxides merged with and underneath the tin features.

The above results are correlated with our previous work on the effect of naphthalene-based additives on tin electrodeposition on gold [10] and boron-doped diamond electrodes[5]. From our previous study using a gold substrate, we demonstrated that NPT and NPTS lie flat on the gold surface and interact mainly via van der Waals forces with the substrate. Furthermore, we showed that NPTS molecules form a more compact structure due to intermolecular lateral interactions. Voltammetric profiles in the presence of NPT and NPTS revealed that NPTS decreases to a higher degree the tin bulk deposition on an iron electrode than NPT, as expected, considering the formation of a more compact film due to intermolecular interactions. Moreover, in spite of the remarkable differences between gold, BDD and iron

substrates, since NPT and NPTS interact mainly via van der Waals forces with the substrate, interactions with the iron electrode surface might not drastically change, neither the intermolecular interactions.

Furthermore, we previously showed that HNPTS molecules do not lie flat on the gold surface, but rather the naphthol group undergoes oxidative polymerization, and such film formation is likely to be formed on other substrates as well since polymerization is not highly sensitive to the electrode surface. Our results of tin electrodeposition on an iron electrode show that HNPTS exhibits a stronger effect on the reduction of tin electrodeposition than NPTS and NPT, similarly to the effect observed on tin electrodeposition on BDD electrode. Additionally, we can see in Figures 5a, 6a and 7a that the cathodic limiting currents in the mass transport control region do not change in the presence of the different concentrations of NPT, NPTS and HNPTS suggesting that Sn (II) ions transport from the bulk to the electrode surface is not affected.

5.3.3 The effect of α-ethoxylated naphthalenesulfonic acid (ENSA -6) on tin electrodeposition on an iron electrode

Figure 8a shows the cyclic voltammograms of tin deposition and dissolution in the presence of ENSA-6. Voltammograms exhibit a strong decrease in the cathodic wave and the plateau correlated to tin deposition. This decrease in the cathodic currents is ascribed to the reduction in the transport of tin (II) ions to the electrode surface, previous studies suggested the complex formation between tin (II)-ENSA [11, 2], but no direct evidence of the complex formation has been confirmed. A decrease of Sn (II) reduction as a consequence of slow mass transport of Sn (II) ions through an ENSA film on the electrode surface is likely. Moreover, a strong decrease and shift to more positive potentials of the peak correlated to the stripping of the tin bulk deposited are observed. The decrease in the anodic peak is a consequence of a lower amount of tin deposited and the shift in the Sn stripping peak is not strongly affected by the rotation rate. However, the reason for this phenomenon requires further study.

Figure 8c and 8d show clear differences of the tin deposits in the absence and presence of ENSA. In the presence of ENSA-6, the electrode exhibits almost no-tin features over the entire surface and the surface shows the characteristic 3D-needle of iron-oxide structures. Nonetheless, Figure 8c shows that the 3D-needles of iron oxides are covered by a blurry structure.

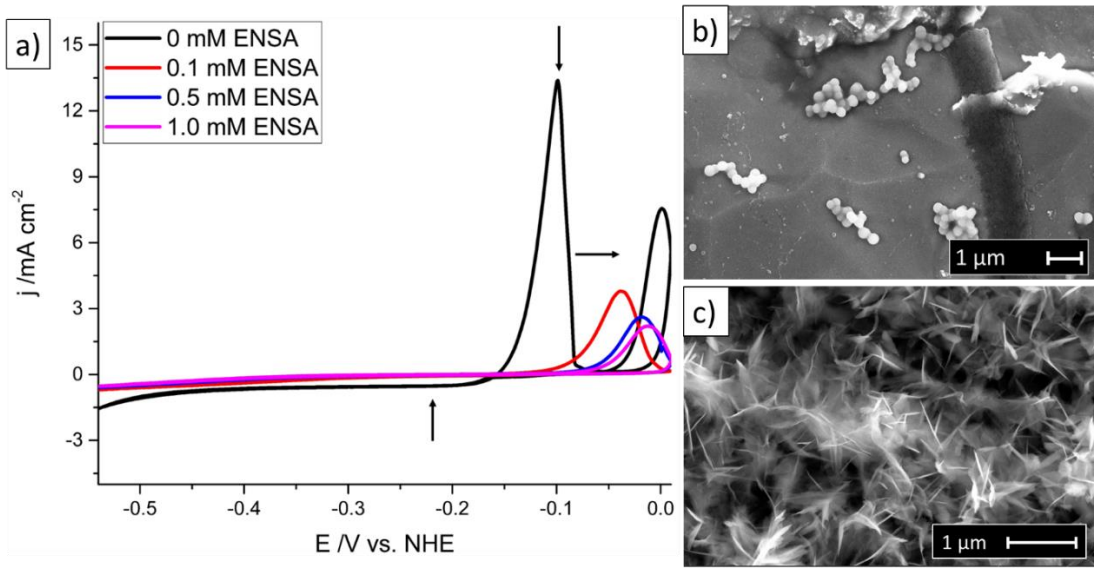

Figure 8. (a) Cyclic voltammograms of tin electrodeposition on a polycrystalline iron RDE, 0.1 M H_2SO_4 at different concentrations of ENSA, recorded between -0.541 to 0.1 V and 30 mV s^{-1} and 1600 rpm. SEM micrographs of tin electrodeposited, on polycrystalline iron; potential was swept from 0.1 to -0.241 V at 30 mV s^{-1} and 1600 rpm, subsequently the potential was held at -0.241 V during 1 minute, 0.1 M H_2SO_4 , 0.6 mM $SnSO_4$: (b) without ENSA (c) with 200 µM ENSA

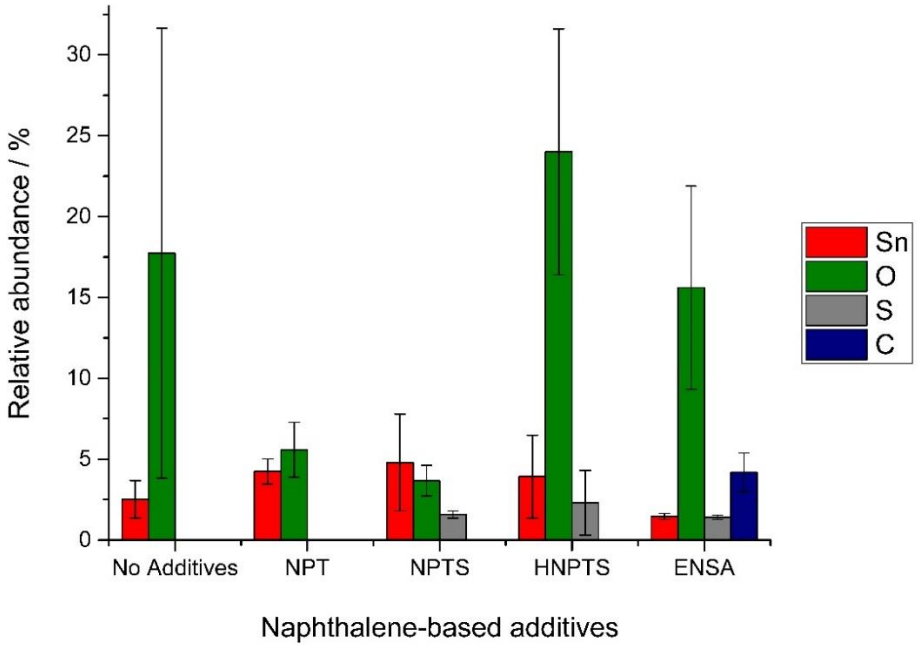

Figure 9. Comparison of relative abundance of the elemental composition for each additive from the EDS measurements. Percentage was calculated from the average of the relative ratio of the different elements in a line scan measurement of about ~0.5 µm length, over the tin features.

Energy dispersive X-ray spectroscopy (EDS) measurements were taken in order to know the elemental composition of the tin deposits grown on the iron electrode in the absence and presence of the different additives. Figure 9 shows that every tin deposit exhibits at least 4% of oxygen content. Additionally, tin deposits in the presence of NPT and NPTS exhibit the lowest amount of oxygen on the surface. Further, tin deposit grown in the presence of ENSA-6 exhibits the lowest amount of tin content (~1.5 %) in accordance with the voltammetric profile (Fig.8a). Besides, a noticeable percentage of carbon and oxygen over the surface is present, which agrees with the ENSA-6 film formation over the tin-iron surface that is observed as a blurry structure on the scanning electron micrographs.

5.4 Conclusions

In this chapter, tin electrodeposition on iron electrodes has been shown to be highly affected by the presence of naphthalene-based additives. We showed the effect of NPT and NPTS on tin electrodeposition remains mainly independent of the substrate. HNPTS shows a stronger decrease of tin deposition, in agreement with has been previously observed on tin deposition on a BDD electrode. Furthermore, we showed that transport of Sn (II) ions from the bulk to the electrode surface is not affected by NPT, NPTS and HNPTS. Lastly, ENSA-6 exhibited the strongest inhibition of tin deposition on iron, an identical observed behavior on gold and BDD. Furthermore, in the presence of ENSA-6 a reduction in the transport of tin (II) ions to the electrode surface was observed; a slow mass transport of Sn (II) ions through an ENSA film on the electrode surface is likely.

5.5 References

(1) Walsh, F. C.; Low, C. T. J. A Review of Developments in the Electrodeposition of Tin. *Surf. Coatings Technol.* 2016, *288*, 79–94. https://doi.org/10.1016/j.surfcoat.2015.12.081.

(2) Van Velzen, C.J; Sluyters-Rehbach, M; Sluysters, J. H. The Electrochemical Reduction of Sn (II) at the Dropping Mercury Electrode from Aqueous 1 M Sulfuric Acid and from 0.3 M Phenolsulphonic Acid and Its Inhibition by ENSA -6. *Electrochim. Acta* 1987, *32* (5), 815–821.

(3) Lee, J.-Y.; Kim, J.-W.; Chang, B.-Y.; Tae Kim, H.; Park, S.-M. Effects of Ethoxylated α-Naphtholsulfonic Acid on Tin Electroplating at Iron Electrodes. *J. Electrochem. Soc.* 2004, *151* (5), C333–C341. https://doi.org/10.1149/1.1690289.

(4) Aranzales, D.; Briliani, I.; McCrum, I. T.; Wijenberg, J. H. O. J.; de Vooys, A. C. A.; Koper, M. T. M. The Effect of Naphthalene-Based Additives on Tin Electrodeposition on a Gold Electrode. *Electrochim. Acta* 2021, *368*, 137606. https://doi.org/10.1016/j.electacta.2020.137606.

(5) Aranzales, D.; Wijenberg, J. H. O. J.; Koper, M. T. M. The Effect of Naphthalene-Based Additives on the Kinetics of Tin Electrodeposition on a Boron Doped Diamond Electrode.

(6) Bockris, J. O. M.; Drazic, D.; Despic, A. R. The Electrode Kinetics of the Deposition and Dissolution of Iron. *Electrochim. Acta* 1961, *4* (2–4), 325–361. https://doi.org/10.1016/0013-4686(61)80026-1.

(7) Bockris, J. O.; Kita, H. Analysis of Galvanostatic Transients and Application to the Iron Electrode Reaction. *J. Electrochem. Soc.* 1961, *108* (7), 676. https://doi.org/10.1149/1.2428188.

(8) Bockris, J. O. M.; Drazic, D. The Kinetics of Deposition and Dissolution of Iron: Effect of Alloying Impurities. *Electrochim. Acta* 1962, *7* (3), 293–313. https://doi.org/10.1016/0013-4686(62)87007-8.

(9) Kelly, E. J. The Active Iron Electrode, I. Iron Discussion and Hydrogen Evolution Reactions in Acidic Sulfate Solutions. *J. Electrochem. Soc.* 1960, *112* (12), 1256. https://doi.org/10.1149/1.2423430.

(10) Aranzales, D.; Briliani, I.; McCrum, I. .; Wijenberg, J. H. O. .; Vooys, De, A. C. A.; Koper, M. T. M. The Effect of Naphthalene-Based Additives on Tin Electrodeposition on a Gold Electrode. *Electrochim. Acta* 2020.

(11) Lee, J.-Y.; Kim, J.-W.; Chang, B.-Y.; Tae Kim, H.; Park, S.-M. Effects of Ethoxylated α-Naphtholsulfonic Acid on Tin Electroplating at Iron Electrodes. *J. Electrochem. Soc.* 2004, *151* (5), C333. https://doi.org/10.1149/1.1690289.